Argon Pumpout by ICRF Waves in C-Mod L- and I-mode Plasmas

J.E. Rice, Y. Lin, C.J. Perks, M.L. Reinke[†], E.S. Marmar,

N. Cao[♯], C. Gao[♮], F. Sciortino[♭], S.J. Wukitch and J. Wright

PSFC, MIT, Cambridge, Massachusetts 02139, USA

[†]*CFS, Cambridge, Massachusetts 02139, USA*

[♯]*CIMS NYU, New York, New York 10012, USA*

[♮]*present address J.P Morgan Chase & Co, New York, New York, USA*

[♭]*IPP Garching 85748, Germany*

Abstract

Pumpout of argon ions by ICRF waves has been observed in C-Mod deuterium L- and I-mode plasmas that had a substantial hydrogen fraction. The effect is manifested by a reduction of core argon x-ray brightness up to a factor of 90% on time scales of tens of milliseconds following injection of ICRF power. For Ar^{16+}, the pumpout is strongest for hydrogen minority concentrations between 0.25 and 0.4, when the ICRF waves are not expected to result in minority heating. Modeling with the TORIC code suggests that the pumpout process occurs when the H/D mode conversion layer overlaps with the 2^{nd} harmonic impurity resonance layer. The magnitude of the argon pumpout is independent of ICRF power above an apparent threshold of $\sim$500 kW, independent of electron density and appears to decrease as the plasma current is increased. Potential application as a heavy impurity control tool in reactors is discussed.

1. Introduction

Contamination of tokamak plasmas by impurities can lead to unwanted radiation losses and dilution of the main ions. In current and future devices with tungsten plasma facing components, it is of crucial importance to keep the plasma tungsten concentration below 10^{-5} n_e. This problem is especially concerning in H-mode discharges where core impurity accumulation is commonly observed. There are several methods that have been employed to remove or screen impurities from the plasma such as the use of divertors, boronization of plasma facing surfaces or utilizing on-axis RF heating schemes. The latter is believed to operate through a change of the electron temperature gradient and has been observed in C-Mod [1] and JET [2] with ion cyclotron range of frequencies (ICRF) waves and in AUG [3] and DIII-D [4, 5, 6] with electron cyclotron heating. A method of directly expelling selected impurities (argon) with ICRF waves has been demonstrated in TFR plasmas [7] through power absorption at the $2^{\rm nd}$ harmonic impurity resonant layer, and that concept will be expanded upon here, in both L- and I-mode discharges. This effect has not been observed in H-mode plasmas, presumably due to strong changes in impurity transport and the fact that to achieve H-mode with ICRF in H minority D discharges, the hydrogen fraction is too low for pumpout in argon, as will be discussed in detail below.

The experimental setup will be described in section 2. In section 3 will be presented the basic observation of argon pumpout, where time histories and radial profile evolution will be discussed. Detailed scalings of the magnitude of the pumpout effect with several plasma parameters will be shown in section 4, including the H to D density ratio, ICRF power, electron density and plasma current. A discussion of ICRF modeling will be given in section 5, along with potential application for tungsten pumpout in reactor grade plasmas.

2. Experimental Setup

The results presented here were obtained from the Alcator C-Mod tokamak [8, 9], a compact (major radius R = 0.67 m, minor radius $a \sim 0.21$ m, typical elongation 1.6), high magnetic field ($B_{\rm T} \leq 8.1$ T) device with molybdenum plasma facing components. For the plasmas described here, the magnetic field ranged from 4.1 to 6.4 T (with a large majority of discharges 5.2-5.5 T) and the plasma current from 0.6 to 1.2 MA (with a large majority 0.8-1.0 MA), with forward and reversed $B_{\rm T}$ and $I_{\rm P}$ in the lower, upper and double null (DN) configurations. Favorable drift refers to the ion $B\times\nabla B$ drift direction towards the X-point, with unfavorable drift away from the X-point. Most of the discharges presented here had average electron densities between 0.7 and 2.2 $\times$ 10^{20}/m^3. The primary auxiliary heating method was with ICRF waves, usually with a hydrogen (H) minority in deuterium (D) plasmas. Two 2-strap antennas operating at 80 MHz delivered power up to 2 MW while a 4-strap antenna provided additional power up to 2 MW at 78 MHz [10], for a total combined power range between 0.2 and 4.0 MW. The D(H) minority heating scheme is most efficient with the n_H/n_D ($\equiv$ H/D, the hydrogen fraction) ratio below 5% [11]. Following openings of the vacuum vessel

at the start of experimental campaigns, the hydrogen level is high after exposure to the water vapor in the air and/or from use of hydrocarbon compounds for cleaning in-vessel components. Typically there are numerous conditioning run days used for reducing the H level in a fairly tedious manner. The H/D ratio was determined by measuring the brightness ratio of the H Balmer α transition at 6562.793 Å to the D transition at 6561.032 Å using a modified Ebert spectrometer [12]. This is a chord averaged measurement dominated by emission from the plasma periphery and may or may not be indicative of the H/D ratio near the plasma center. For the discharges studied here, the H/D ratio was in the range from 0.01 to 1.5. The quantity H/H+D will be used in the following since it is a good approximation to n_H/n_e ($\equiv$ hydrogen concentration), and its values range from 0 to 1. Pumpout of argon was primarily measured using x-ray transitions from He-like Ar^{16+} (the forbidden line z, $1s^2\ ^1S_0$ - $1s2p\ ^3S_1$ at 3994.28 mÅ [13]) and H-like Ar^{17+} (the Ly_α doublet, $1s\ ^1S_{1/2}$ - $2p\ ^2P_{3/2}$ at 3731.10 mÅ and $1s\ ^1S_{1/2}$ - $2p\ ^2P_{1/2}$ at 3736.52 mÅ [14]). Line of sight integrated x-ray spectra were obtained from a spatially imaging spherical crystal Johann spectrometer system [15, 16] (quartz 102 crystals, 2d = 4562.15 mÅ). The resolving power was $\lambda/\Delta\lambda \sim$ 5000 (with typical integration time of 20 ms). Argon was introduced into the plasma through a piezo-electric valve and the ambient level, with core concentrations typically between 10^{-3} and 10^{-4} n_e, was usually maintained by recycling. Molybdenum is a naturally occurring impurity in C-Mod and since the 4D transition in Mo^{32+} at 3739.8 mÅ [17] falls in the same spectral range as the H-like Ar^{17+} Ly_α doublet, information about potential molybdenum pumpout can be ascertained. Possible pumpout of other impurities can be addressed through transitions which can be observed with a pair of VUV spectrometers [18].

3. Observations of Argon Pumpout by ICRF Waves

The basic pumpout effect is depicted in Fig.1 which shows parameter time histories for a 5.4 T, 1.0 MA discharge with unfavorable drift and H/H+D $\sim$0.33 (H/D $\sim$0.49). 0.5 MW of ICRF power at 80 MHz were delivered between 1.0 and 1.5 s, and with such a high hydrogen fraction, there was very little effect on the electron temperature [11] (or density). There was a very large effect on the brightness of argon transitions, with strong pumpout of $\sim$65% for Ar^{16+}, which evolved on a time scale of $\sim$45 ms, about a factor of 2 longer than a typical impurity confinement time in L-mode [19]. Since neither the electron temperature nor the electron density changed during the ICRF power injection, the drop in argon brightness can be attributed to a drop in argon density. In contrast, the Mo^{32+} signal increased during this time. This may be due to an increase in the edge source of molybdenum during the ICRF wave injection [20]. This increase in molybdenum did not affect plasma performance, as the stored energy and H-factor remained unchanged. (Other impurities will be discussed in the next section.) Examination of the bottom frame, which includes both central and edge views of the Ar^{16+} forbidden line, reveals that the percentage drop in signal is stronger at the mid radius, which will be discussed anon. In order to demonstrate that the drop in argon brightness is due to ICRF waves, consider Fig.2, which compares parameter time histories

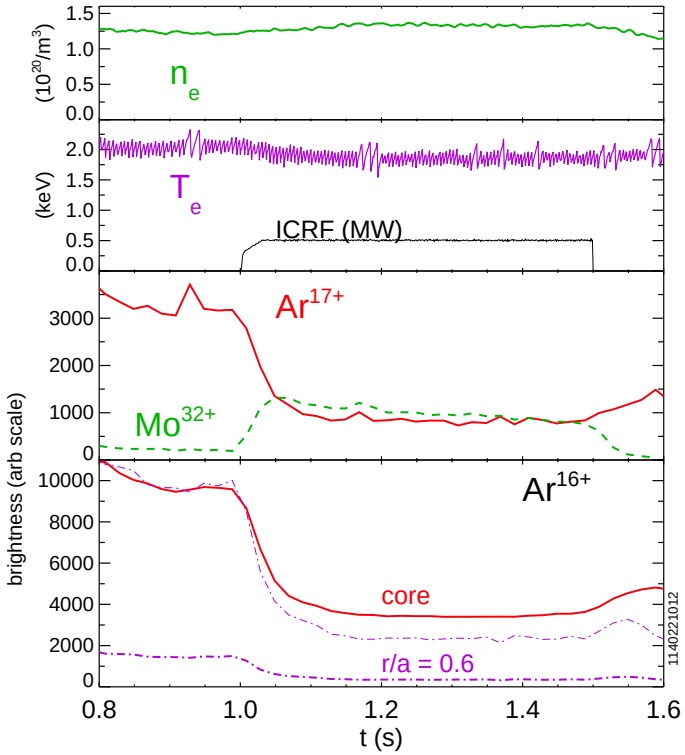

Figure 1: Parameter time histories for a 5.4 T, 1.0 MA L-mode discharge with unfavorable drift and H/H+D ∼0.33. Top frame, the average electron density; second frame, the central electron temperature (and ICRF power); third frame, the central chord brightnesses of Ar^{17+} (solid red) and Mo^{32+} (dashed green); bottom frame, brightness of Ar^{16+} with a central view (solid red) and through r/a ∼0.6 (dash-dot purple). The light dash-dot purple line in the bottom frame is normalized to the central view before the ICRF.

of two successive discharges with different ICRF waveforms. Both plasmas exhibited

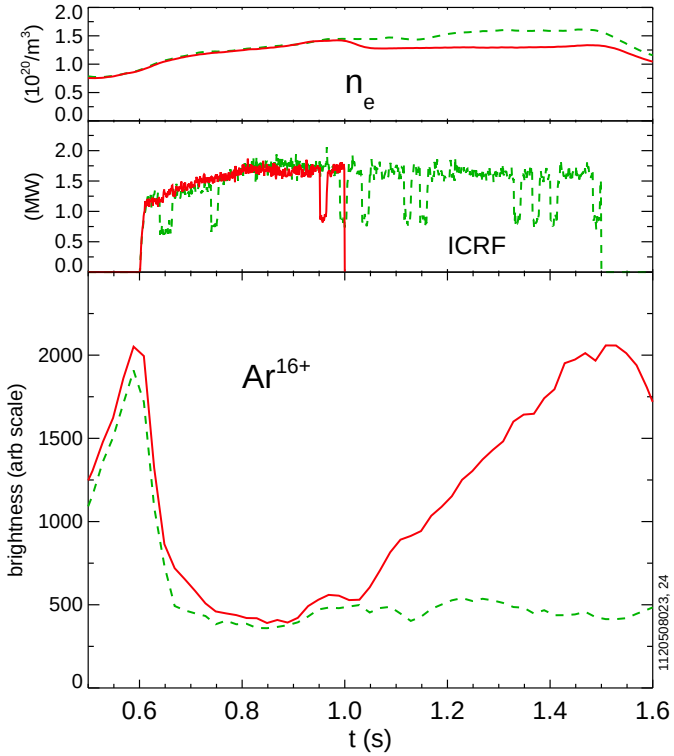

Figure 2: A comparison of the time histories (from top to bottom, the electron density, ICRF power and Ar^{16+} brightness) of two successive 5.5 T, 0.8 MA discharges with unfavorable drift and H/H+D $\sim$0.28, that had different ICRF waveforms.

a rapid decrease in the argon brightness immediately following ICRF power injection, but in the case with the early termination, the argon signal rose to its previous level. As was alluded to in Fig.1, the pumpout effect appears larger outside of the plasma core. Shown in Fig.3 is the ratio of Ar^{16+} brightness profiles obtained during and before the ICRF wave injection for the plasma of Fig.1. The pumpout is larger in the outer half of the plasma with the maximum effect close to the location of the Ar^{16+} $2^{\rm nd}$ harmonic resonant layer location indicated by the vertical line. This will be discussed in detail in section 5.

4. Parameter Scaling of Argon Pumpout

This section will examine the parameter scalings of the pumpout effect. The argon line brightnesses will serve as a measure of the pumpout, as a proxy for the argon den-

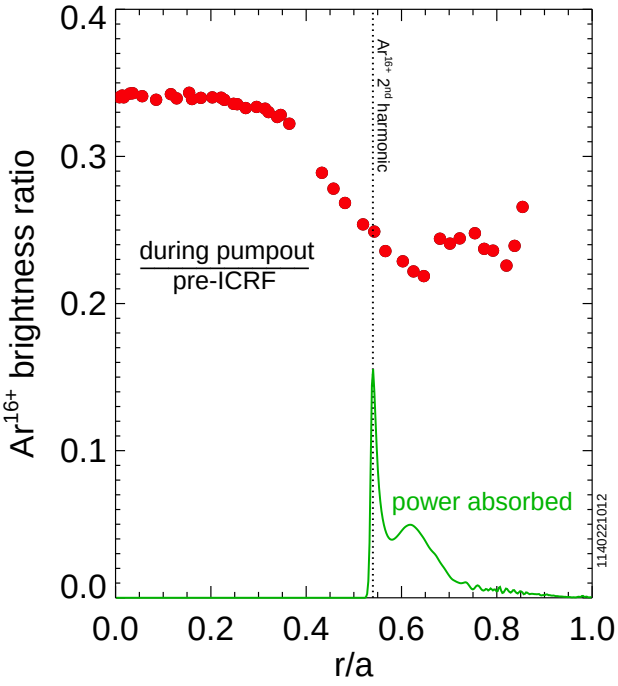

Figure 3: The red dots represent the ratio of the radial Ar^{16+} brightness profiles during the pumpout and before the ICRF for the discharge of Fig.1. The dotted vertical line indicates the location of the Ar^{16+} 2^{nd} harmonic resonant layer. The green curve represents the calculated power absorption profile for Ar^{16+} ions (units given in Fig.19) and will be discussed in detail in Section 5.

sity. A database of ∼400 discharges has been assembled from numerous ICRF antenna conditioning runs. A large majority of these plasmas had a magnetic field between 5.2 and 5.5 T, with plasma currents between 0.8 and 1.0 MA. The hydrogen level was generally not actively controlled, and values of H/D varied from 1.5 immediately following vacuum breaks to as low as 0.01 following boronization. H/H+D in these experiments ranged from 0.01 to 0.58. The most important parameter for the pumpout effect turns out to be hydrogen level, as demonstrated in Fig.4, which shows the change in the Ar^{16+} brightness ($\Delta Br_{16+} \equiv [Br_{16+pre-ICRF} - Br_{16+duringICRF}]/Br_{16+pre-ICRF}$, the difference in the argon brightness before and during the ICRF, normalized to the brightness before) as a function of the hydrogen concentration, H/H+D. Inspection of

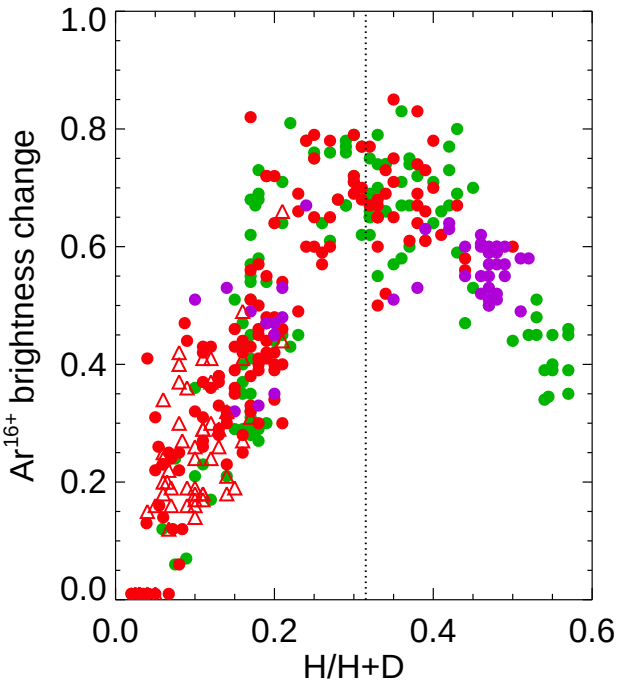

Figure 4: The change in the Ar^{16+} brightness as a function of H/H+D. Dots are from L-mode discharges: green for favorable drift, red for unfavorable drift and purple for double null. Triangles are from I-mode plasmas. The vertical dotted line is for H/H+D = 0.31 (H/D = 0.46).

the figure reveals that the pumpout is largest (between 60 and 80%) for H/H+D values between 0.25 and 0.4, and that the points are intermixed, indicating no dependence on magnetic configuration. The dots represent points from L-mode plasmas, and the I-mode discharges (triangles) overlap. (I-mode [21, 22] is a confinement regime formed

with unfavorable drift, which features the energy confinement properties of H-mode and the particle and impurity [19] confinement characteristics of L-mode.) H-mode discharges do not show any pumpout as the argon brightnesses increase strongly, from an inward impurity pinch due to the steep pedestal density gradient [19]. H-mode is usually only accessed with hydrogen fractions below 10%. The pumpout effect is quite small for the lowest values of H/H+D. There is substantial scatter in the plot, which can be from a variety of causes: different plasma shapes and outer gaps, changes in the electron temperature, different values of $Z_{\rm eff}$, low visible light levels which lead to large error bars in H/H+D, changes in the H/D ratio during the ICRF pulse, *etc*. The vertical line at H/H+D = 0.31, which is close the pumpout maximum, will be discussed in the next section.

Since the pumpout effect was also observed in Ar^{17+} as was seen in Fig.1, it is possible to construct a similar scaling, and the results are demonstrated in Fig.5. For

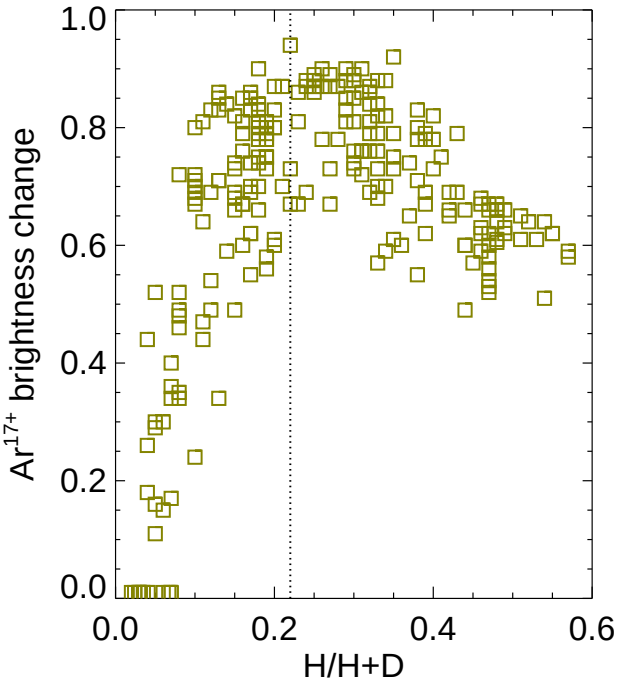

Figure 5: The change in the Ar^{17+} brightness as a function of H/H+D. The vertical dotted line is for H/H+D = 0.22 (H/D = 0.29). These points are not sorted by magnetic configuration.

Ar^{17+}, the maximum pumpout ranges from 70 to 90%, and occurs for slightly lower values of H/H+D compared to Ar^{16+}, between 0.15 and 0.35. The points in Fig.5

are not sorted by magnetic configuration since there is no apparent dependence. The vertical line with H/H+D = 0.22 will be discussed in the next section. No pumpout effect was observed for Mo^{32+} over this range of H/H+D; in fact in all discharges there was an increase in the molybdenum brightness during the ICRF wave injection, including in Mo^{30+}, as seen in Fig.6 (third panel). A similar increase was seen from

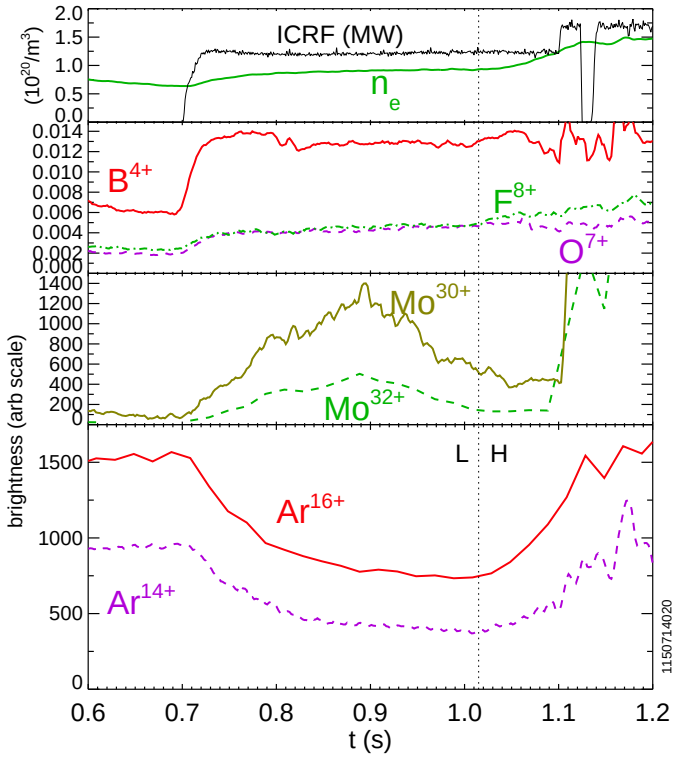

Figure 6: Brightness time histories for several impurity transitions from a 5.4 T, 0.9 MA discharge with favorable drift and H/H+D = 0.15. In the top panel are shown the electron density and ICRF waveform; in the 2nd panel brightnesses from the hydrogen-like ions B^{4+} (solid red line, BV at 48.95 Å), O^{7+} (purple dashed line, OVIII at 18.97 Å) and F^{8+} (green dash-dot line, FIX at 14.99 Å); 3rd frame Mo^{32+} (green dashed line) and magnesium-like Mo^{30+} (solid mustard line, MoXXXI at 115.99 Å); bottom frame Ar^{16+} (red line) and Be-like Ar^{14+} (purple dashed line at 22.15 Å). This plasma entered H-mode at 1.015 s.

intrinsic low Z impurity species, and an example is shown in the second panel. Argon pumpout was observed between 0.7 and 1.0 s in the two charge states shown in the bottom panel. Following 1.015 s when the plasma entered H-mode, the argon signals increased, along with the electron density. The line brightnesses from other impurity species all increased after 0.7 s during the argon pumpout following ICRF wave in-

jection. Data from Be-like Ar^{14+} (221.19 Å, bottom frame) were only available for a subset of discharges in the database, and were rarely available for Li-like Ar^{15+} (23.5 Å). Still, it was possible to obtain some information of the pumpout scaling for Ar^{14+} and the results are shown in Fig.7. There is considerably more scatter compared to

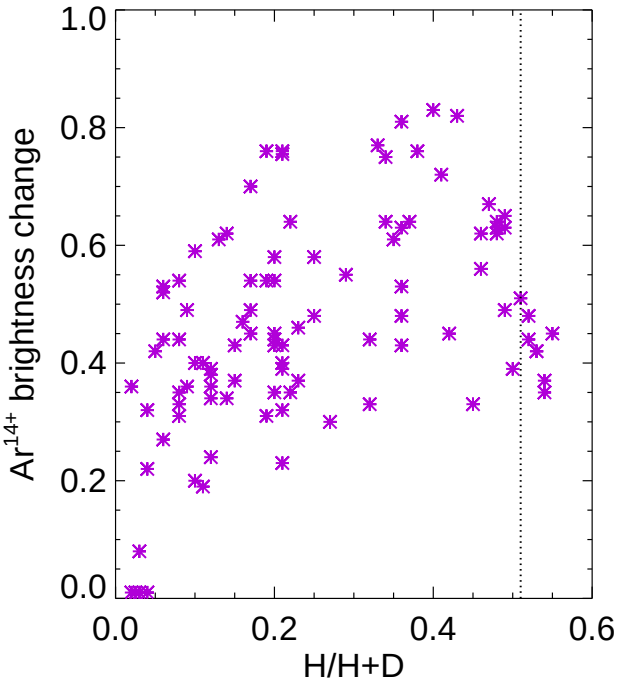

Figure 7: The change in the Ar^{14+} brightness as a function of H/H+D. The vertical dotted line is for H/H+D = 0.51 (H/D = 1.05).

Figs.4 and 5, and no maximum with H/H+D stands out. The vertical line with H/H+D = 0.51 will be discussed in the next section. A comparison of Figs.4, 5 and 7 indicates that the magnitude of maximum pumpout decreases as the charge state increases, going from ∼80% for Ar^{17+} to ∼70% for Ar^{16+} to ∼55% for Ar^{14+}.

Since the pumpout is associated with ICRF waves, it is natural to expect a relation with the injected power and a possible threshold for the effect. The pumpout was observed in Fig.1 with only 500 kW. This question is explored in Fig.8 in which there was a step in ICRF power. Clearly there is evidence of the pumpout effect between 0.6 and 1.0 s when the ICRF power was 0.28 MW, but that the effect was stronger between 1.0 and 1.5 s with 0.81 MW of power. Contrast this result, along with Figs.1 and 2, with the discharge shown in Fig.9. In this case with 1.15 MW of ICRF power between 0.6 and 0.73 s, no pumpout was observed, while at the same time there was an increase

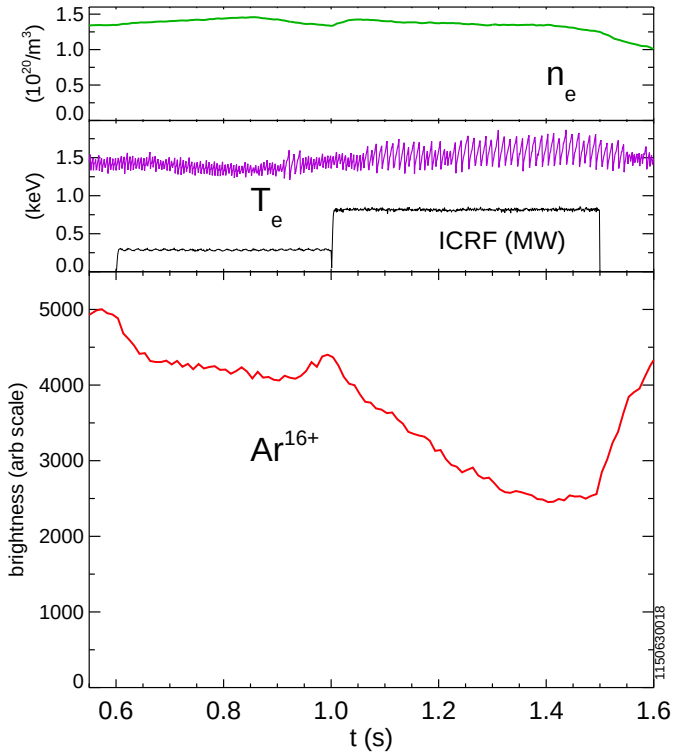

Figure 8: Parameter time histories of a 5.4 T, 1.0 MA discharge with unfavorable drift and H/H+D $\sim$0.4.

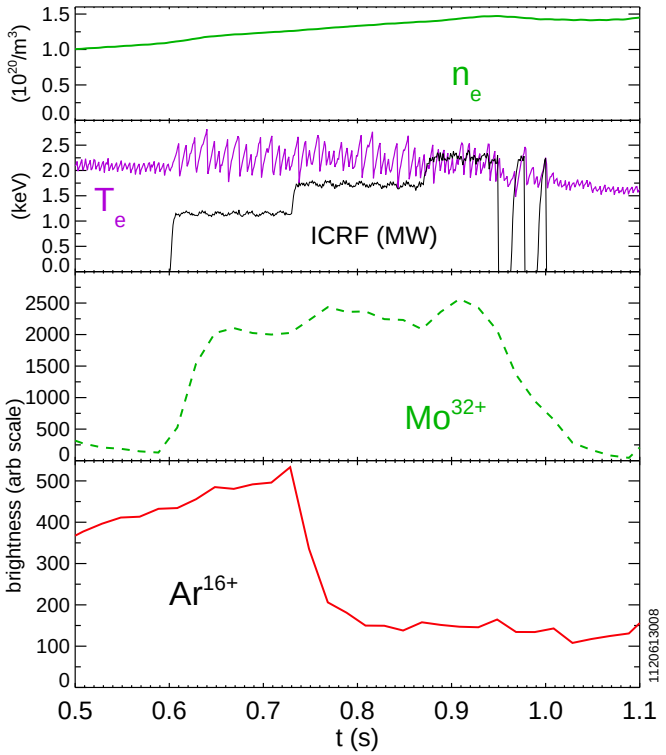

Figure 9: Parameter time histories of a 5.2 T, 0.8 MA discharge with favorable drift and H/H+D = 0.098.

in the Mo^{32+} signal as was seen in Fig.1. Following the step to 1.75 MW at 0.73 s, the pumpout initiated, and there was no further reduction in signal after the 3rd step to 2.25 MW at 0.87 s. This behavior has only been observed in discharges with very low H/H+D, in this case ∼0.1, and as was seen in Fig.4, the pumpout effect is weak with these low values. Comparison of Figs.8 and 9 indicates that the power threshold for pumpout may depend upon the H/D ratio since there is a lot of scatter at low H/H+D as was seen in Fig.4. Additionally, it should be noted that the pumpout effect is observed even with an irregular waveform, as demonstrated in Fig.10. In spite of substantial

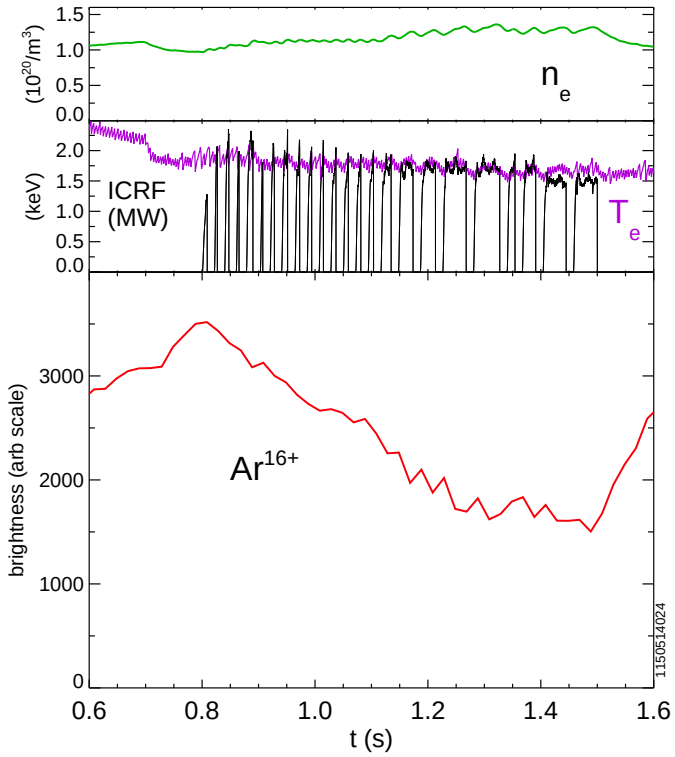

Figure 10: Parameter time histories of a 5.4 T, 0.8 MA discharge with unfavorable drift and H/H+D = 0.34.

intermittency in the ICRF power, a clear pumpout effect was observed.

The change in the Ar^{16+} brightness as a function of ICRF power is shown in Fig.11 for numerous individual discharges with $0.2 < \text{H/H+D} < 0.4$. These plasmas represent favorable and unfavorable configurations, with plasma currents between 0.8 and 1.0 MA and with electron densities from 1.0 to 1.6 $\times 10^{20}/\text{m}^3$. Above an apparent threshold of ∼500 kW, the magnitude of the pumpout effect is independent of ICRF power. A similar independence is seen for lower values of H/H+D, as can be seen in Fig.12. In these cases, the magnitude of the pumpout is lower and there is considerably more

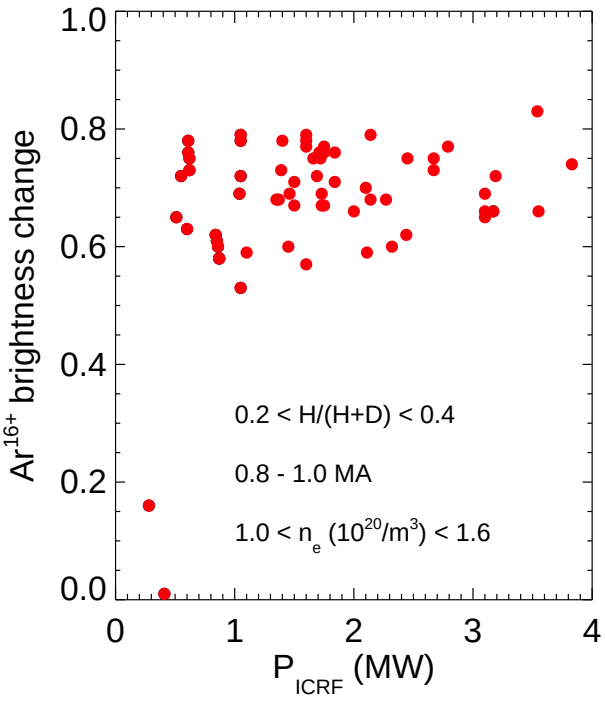

Figure 11: The change in the Ar^{16+} brightness as a function of ICRF power, for favorable, unfavorable and double null discharges with $0.2 <$ H/H+D < 0.4, plasma currents from 0.8 to 1.0 MA and electron densities between 1.0 and $1.6 \times 10^{20}/m^3$.

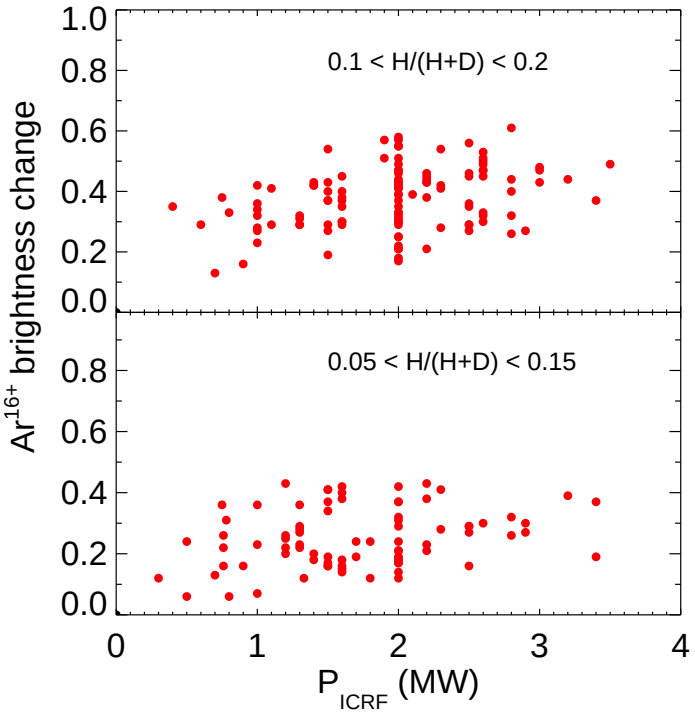

Figure 12: The change in the Ar^{16+} brightness as a function of ICRF power for discharges with $0.1 < H/H+D < 0.2$ (top frame) and $0.05 < H/H+D < 0.15$ (bottom frame).

scatter. The pumpout relation with electron density has been explored in discharges with H/H+D between 0.2 and 0.4, and the results are shown in Fig.13. The effect is

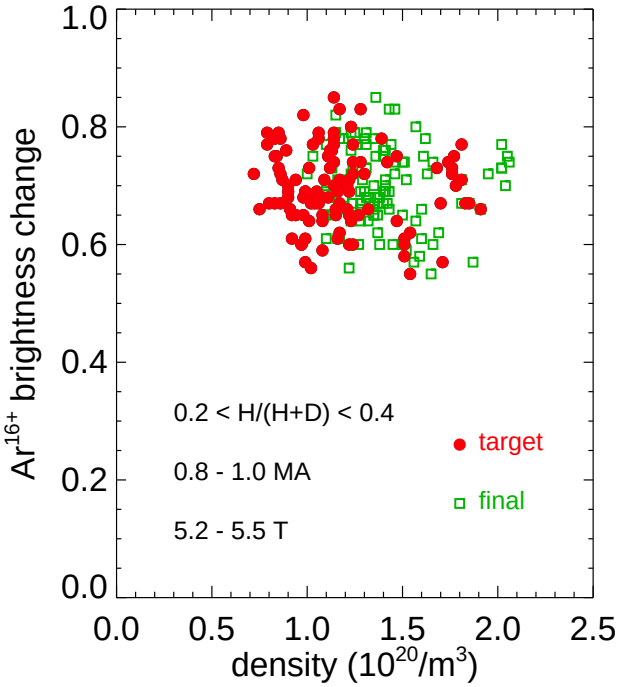

Figure 13: The change in the Ar^{16+} brightness as a function of electron density (red dots for target and green squares for final) for discharges with 0.2 < H/H+D < 0.4.

independent of density over this range, either in the target value (red dots) or in the final level (green squares) during the ICRF wave injection.

As was mentioned earlier, the large majority of discharges was with plasma currents between 0.8 and 1.0 MA. This range was expanded in some cases with H/H+D between 0.05 and 0.1, well below the optimum values for pumpout (from 0.2 to 0.4); examples of three discharge time histories are shown in Fig.14. The lowest current plasma (0.6 MA) experienced a much stronger pumpout than the one with highest current (1.2 MA). A scaling with the magnitude of the pumpout with plasma current for several similar discharges is shown in Fig.15. There is a substantial drop in the pumpout magnitude with increasing current. Unfortunately, there are no similar cases for a larger range in current at higher values of H/H+D where the pumpout effect is stronger. It was also mentioned earlier that most of the discharges in the database had a central magnetic field between 5.2 and 5.5 T. There are a few examples with B_T outside of this range but it is not possible to obtain a meaningful scaling with magnetic field, although there

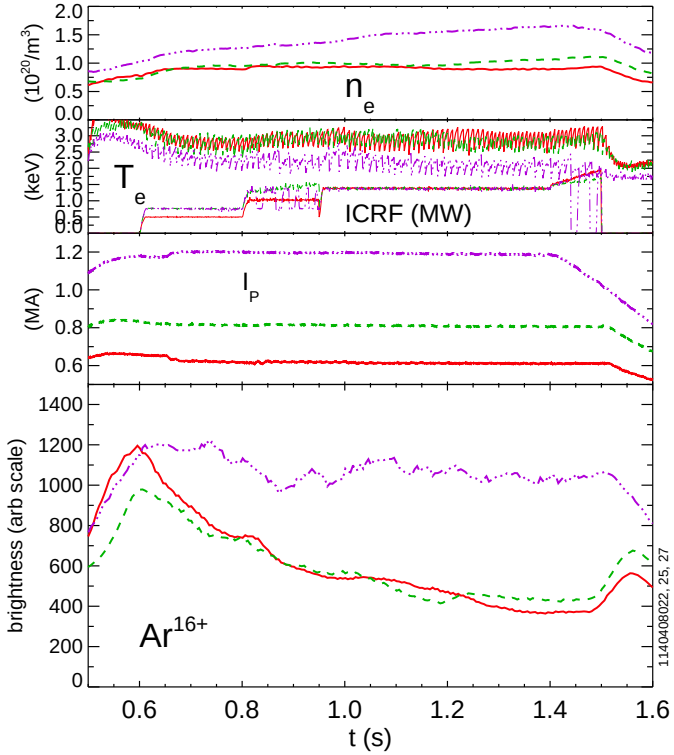

Figure 14: A comparison of the time histories for three 5.4 T, unfavorable drift discharges with H/H+D = 0.05, and similar ICRF waveforms: 1.2 MA- purple dash-dot line; 0.8 MA- green dashed line; 0.6 MA- solid red line.

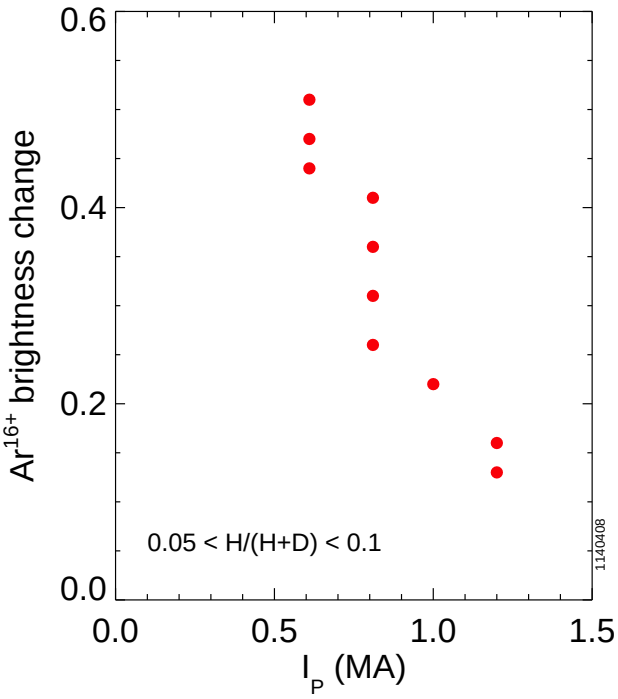

Figure 15: The change in the Ar^{16+} brightness as a function of plasma current for 5.4 T, unfavorable drift discharges with $0.05 < H/H+D < 0.1$.

are indications that if there is any B_T dependence, it is weak.

5. ICRF Modeling, Discussion and Summary

Pumpout of argon ions by ICRF waves was first demonstrated in TFR plasmas [7]. The magnetosonic wave launched by the ICRF antenna can be mode converted (MC) into a quasi electrostatic wave at the two ion hybrid resonant layer [23] located on a vertical chord which depends upon the magnetic field strength, ICRF frequency and H/D ratio, given by

$$R_{MC} = R_0 \frac{eB_0}{m_p \omega_{RF}} \frac{\sqrt{1+\alpha/2}}{\sqrt{1+2\alpha}} \tag{1}$$

where α is the H/D density ratio and R_0 is the device major radius. If this location overlaps with the impurity cyclotron resonance layer, given by

$$R_I = R_0 \frac{eB_0}{m_p \omega_{RF}} nZ/A \tag{2}$$

where n is the harmonic number and Z/A is the impurity charge to mass ratio, the impurity can gain perpendicular energy and be expelled from the plasma [7]. The location of the $2^{\rm nd}$ harmonic resonance layer for Ar^{16+} is shown in Fig.3 by the dotted vertical line, and corresponds to the maximum of the pumpout effect. The layer overlap condition, $R_{MC} = R_I$, is only a function of the H/D density ratio in the plasma and can be expressed as

$$\frac{H}{D} = \frac{1-(nZ/A)^2}{2(nZ/A)^2 - 1/2}. \tag{3}$$

This condition is independent of magnetic field and electron density, in agreement with observations. Of course a necessity for the pumpout effect is that the impurity ion of interest exists at this location in the plasma. Table 1 summarizes the H/D and H/H+D values for overlap with the impurity $2^{\rm nd}$ harmonic for several ions of interest.

For Ar^{16+} with Z/A = 0.40, the layer overlap condition is satisfied for H/H+D = 0.31 and agrees very nicely with the maximum pumpout shown in Fig.4. For Ar^{17+} the H/H+D value is lower, 0.22, and in agreement with the results of Fig.5. For Ar^{14+} the H/H+D value is higher, 0.51, shown by the vertical line in Fig.7. In this case, the H/D ratio obtained was not high enough to exhibit a significant drop in the pumpout effect. Furthermore, the density of Ar^{14+} is very low at the layer overlap location in the plasma, so evidence of the pumpout effect may not be expected. Similarly, as was seen in Fig.6, there was no pumpout observed for B^{4+}, O^{7+} and F^{8+} because these charge states do not exist at the critical layer, and in the case of B^{4+}, H/H+D was too high. The pumpout should occur for fully stripped B^{5+} in the core of plasmas with H/D $\sim$0.1 (ideal for D(H) minority heating) but to observe this would require charge exchange population of transition upper levels. In the cases of the molybdenum ions

ion	Z/A	H/D	H/H+D	existence
B^{4+}	0.37	0.76	0.43	no
B^{5+}	0.46	0.12	0.11	yes
O^{7+}	0.44	0.23	0.19	no
F^{8+}	0.42	0.32	0.24	no
Ar^{14+}	0.35	1.05	0.51	maybe
Ar^{15+}	0.38	0.70	0.41	yes
Ar^{16+}	0.40	0.46	0.31	yes
Ar^{17+}	0.43	0.29	0.22	yes
Mo^{30+}	0.31	2.16	0.68	yes
Mo^{31+}	0.32	1.74	0.64	yes
Mo^{32+}	0.33	1.42	0.59	yes
W^{46+}	0.25	936	0.99	
W^{56+}	0.30	2.59	0.72	
W^{64+}	0.35	1.10	0.52	

Table 1: Various ions and the H/D values for overlap between the MC layer and the second harmonic impurity resonant layer. First column- impurity charge state; second column- charge to mass ratio; third column- H/D (hydrogen fraction); fourth column- H/H+D (hydrogen concentration); last column- does the ion exist at this layer?

in the table, they do exist at the critical layer, but the calculated values of the hydrogen concentration are too high, since H/H+D was below 0.58 for the experiments described here. Another complication with molybdenum is that the ICRF power acts as an edge source, which could mask any potential pumpout effect. Also shown in Table 1 are the entries for tungsten (Z = 74, A = 183.84) ions of interest, including neon-like W^{64+}, argon-like W^{56+} and nickel-like W^{46+}, which are expected to be present in SPARC plasmas [24]. For W^{46+}, which has been observed in AUG plasmas [25], the charge to mass ratio is 0.2502, which is extremely close to 1/4, and renders Eq.3 infinite for n = 2 (H/H+D = 1, a pure hydrogen plasma). Unfortunately for the pumpout to work for W^{64+}, the H/D ratio would have to be of order unity, which is way too high for the D(H) minority heating scheme. The possibility of tungsten pumpout in D/T plasmas with a ^{3}He minority needs to be explored (see below). In fact, ICRF wave absorption was observed in ^{7}Li ions during D/T experiments on TFTR [26].

The above discussion was mainly based on a plausibility argument, without detailed modeling. The TORIC code [27, 28] has been used to provide a more quantitative description of the pumpout process. Simulation shows that indeed the argon ions interact with the RF field. The strongest interaction happens when the impurity $2^{\rm nd}$ harmonic resonance is near the mode conversion layer (ion-ion hybrid layer), where the RF electric field is enhanced and short wavelength slow waves are generated by the mode conversion process. The $2^{\rm nd}$ harmonic $\omega = 2\omega_i$ RF power absorption by argon ions appears to play a major role in the observed argon ion pumpout. The $2^{\rm nd}$ harmonic power absorption is a finite Larmor radius effect: if the wave spatial structure is too large scale compared to the Larmor radius, the acceleration of the particles by the RF

electric field would be cancelled from two consecutive wave periods. The absorption of the RF power at the $2^{\rm nd}$ harmonic resonance is strongly affected by $(k_\perp \rho_i)^2 |E_+|^2$ [29]. E_+ is the electric field that has left-handed polarization and can accelerate the ions at the cyclotron resonance or harmonics (see Fig.16). E_+ is usually small from the natural polarization filtering by the plasma for the fast wave. Therefore for fast wave heating, $2^{\rm nd}$ harmonic heating would only be significant if the $k_\perp \rho_i$ is large, but not arbitrarily so. However, in these cases, $k_\perp \rho_i$ is very small. Increasing this value is required to have absorption (by having larger $k_\perp$ in the MC waves than the fast wave by a factor 5-10). For bulk ion absorption of the fast wave, this requirement is approximately proportional to the ion beta. For typical fast wave heating scenarios, the absorption by argon ions would be too small because of the much smaller ρ_i than the bulk plasma. However, with higher H levels, the heating scenario moves from minority heating to mode conversion (MC) heating. At the location near $n_\parallel{}^2 = S$, where S is one of the Stix parameters, some of the fast wave can be converted to short-wavelength slow waves: Ion Bernstein waves (IBW) on the mid-plane and ion cyclotron waves (ICW) off the mid-plane. Both MC IBW and MC ICW have much smaller $k_\perp$ than the fast wave. Associated with the near resonance condition at the MC layer, the waves also have a much larger E_+ field [30, 31]. As a result, if there is a $2^{\rm nd}$ harmonic resonance of argon ions near the MC layer, the argon ions can strongly interact with the local RF field and get accelerated to high energy, leading to escape from the plasma. Note that $2^{\rm nd}$ harmonic heating is bootstrapping: with higher energy, there is a larger Larmor radius and more absorption, which can generate unconfined particles (pumpout). Note that in the TFR experiment [7], the ICRF antenna was on the high magnetic field side (HFS), and mode conversion to ICW dominated. For the C-Mod case, launching from low magnetic field side (LFS), both MC ICW and IBW exist and can contribute.

In this study, the RF code TORIC [27, 28] has been used to simulate the wave field and the power absorption by argon ions. TORIC is a two-dimensional full-wave ICRF code which solves a $6^{\rm th}$ order wave equation with second order finite Larmor radius terms that can resolve the fast wave and mode converted short-wavelength slow waves. In the mode conversion regime, TORIC has been shown in previous studies [31, 32] to agree reasonably with the experimental measurement of power deposition profiles and power partition among species. Plasma parameters from the discharge shown in Figs.1 and 3 are used in simulation, assuming concentrations of Ar^{16+} and Ar^{17+} = 0.0005 n_e. Because of toroidal symmetry, the electric field of different toroidal modes is not coupled. Each TORIC run computes the RF wave field for a given toroidal number and calculates the power partition among different species and absorption mechanisms. The results from multiple toroidal modes are then summed based on the antenna spectra (calculated based on antenna geometry and phasing) and weighted by equivalent antenna loading for the toroidal mode (also calculated by TORIC). The C-Mod 2-strap antenna spectrum is used for the simulation [31]. Toroidal mode numbers of +10 and -10 were run for the H concentration scan (20% to 40%), and for selected H concentrations, to generate the power deposition profiles, and the entire antenna spectra are simulated and then weight averaged. In the simulations, the H ion temperature is assumed to be the same as the bulk D ion temperature, with Maxwellian distribution functions, and that $T_i = T_e = 1.5$ keV. This assumption would be invalid in the minority heating scenarios with lower H concentrations. To have consistent results, here the

TORIC calculations only cover the range of H concentration from 20% to 40%, where mode conversion heating dominates.

Shown in Fig.16 are the calculated contours of the real parts of the electric field components: E_+, E_- and E_ζ for a C-Mod discharge with H/H+D = 0.30. The IBW

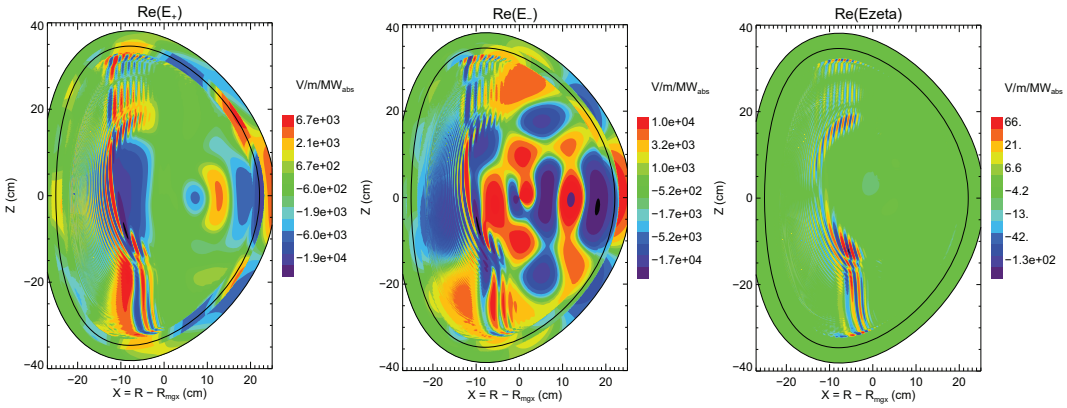

Figure 16: The calculated contours of the real parts of the electric field components: E_+ (left), E_- (center) and E_ζ (right) for a C-Mod discharge with H/H+D = 0.30. The ion-ion hybrid (MC) layer is at X = -11.7 cm.

resides on the mid-plane to the HFS of the hybrid layer and the ICW is above and below the mid-plane to the LFS of the hybrid layer. E_- is the field with right-handed polarization; the fast wave launched from the antenna is mostly E_- field. E_+ is the component of the field with left-handed polarization, which gets strong near the MC layer. E_+ can heat ions if it is also near a cyclotron resonance. E_ζ is a feature of the mode converted slow waves which appears naturally with the MC process.

Contours of power absorption for argon ions of interest with H/H+D = 0.30 and toroidal mode number n_ϕ = 10 are shown in Fig.17. Note that the mode conversion process happens in a finite region in space [32] and so does the $2^{\rm nd}$ harmonic absorption. The absorption is quite complicated: it only happens along the $2^{\rm nd}$ harmonic line and in the region where short wavelength waves with large E_+ exist, as shown in Fig.16. When the $2^{\rm nd}$ harmonic layer is on the HFS of the MC layer, the interaction is more localized near the mid-plane, where the MC IBW propagates toward the HFS and interacts with the Ar ions at the $2^{\rm nd}$ harmonic resonance (the Ar^{16+} case in Fig.17).

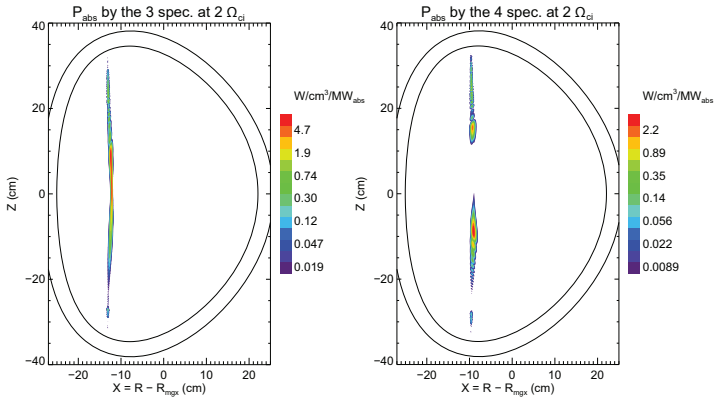

Figure 17: Contours of power absorption for Ar^{16+} (left) and Ar^{17+} (right) for a C-Mod discharge with H/H+D = 0.30 and toroidal mode number n_ϕ = 10. For this setup, the Ar^{16+} 2^{nd} harmonic is at X = -12.1 cm, the Ar^{17+} 2^{nd} harmonic at X = -8.96 cm and the MC layer at X = -11.7 cm. The Ar^{16+} 2^{nd} harmonic resonance is on the HFS of the MC layer and the Ar^{17+} 2^{nd} harmonic resonance is on the LFS of the MC layer.

When the 2nd harmonic layer is on the LFS of the MC layer (larger H concentration), the power absorption is more localized at the intersection of the near vertical 2nd harmonic resonance layer and the flux surface where the MC ICW propagates towards the LFS (Ar^{17+} case in Fig.17).

The hydrogen concentration (∼H/H+D) has a strong effect on power absorption of the ICRF waves, which also depends on the charge to mass ratio of the ion in question. This is demonstrated in Fig.18 which is a plot of the power fraction as a function of H/H+D for Ar^{16+} and Ar^{17+}. The power to the Ar ions is low, but clearly there

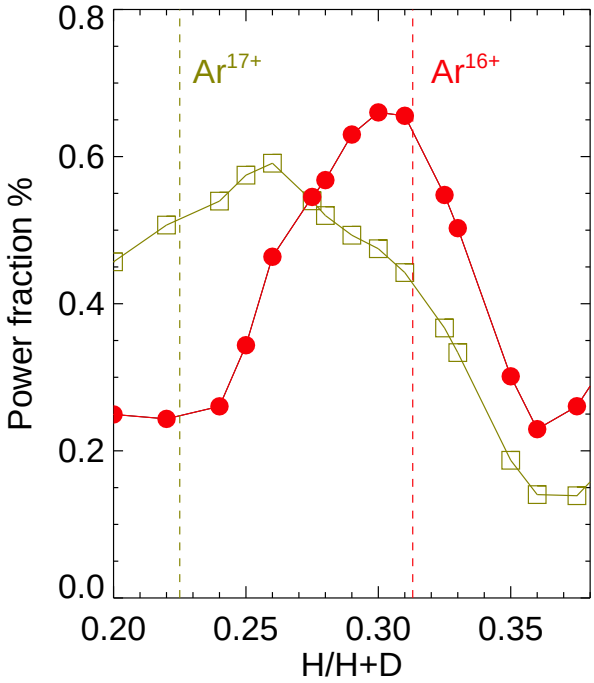

Figure 18: The calculated power fraction as a function of hydrogen concentration for Ar^{16+} (red dots) and Ar^{17+} (mustard squares). The vertical lines represent the values calculated from Eq.3, and shown in Figs.4 and 5.

is a peak around H/H+D = 31% for Ar^{16+} and around H/H+D = 22% for Ar^{17+}, in accordance with Eq.3 and Table 1. This power level is significant because the absolute argon concentration is so low. These calculations are in excellent qualitative agreement with the observations shown in Figs.4 and 5.

As was seen in Fig.17, there are very narrow vertical bands where the 2nd harmonic impurity layers exist, and as such, the absorbed power can also be spatially localized. This is presented in Fig.19 which shows the calculated power deposition radial pro-

files for different values of the hydrogen concentration. The power deposition profiles

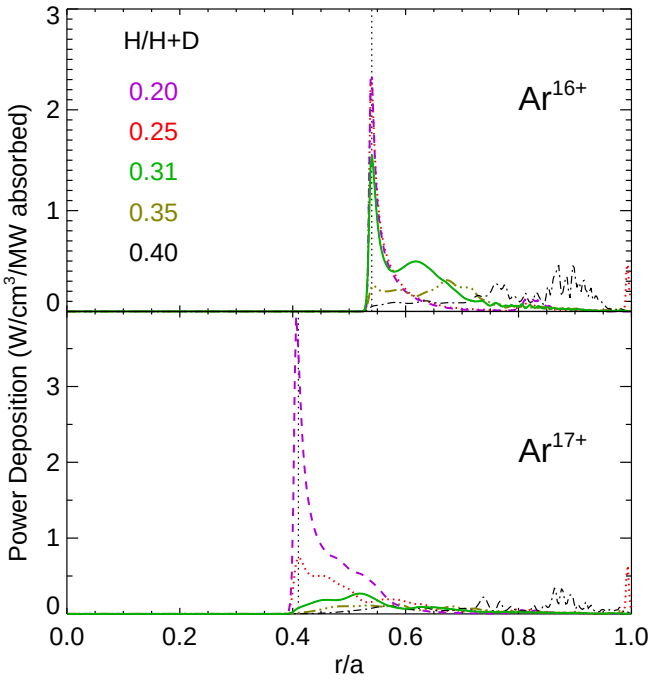

Figure 19: The power deposition profiles for Ar^{16+} (top) and Ar^{17+} (bottom), with different values for H/H+D: 0.20, purple dashed line; 0.25, dotted red line; 0.31, solid green line; 0.35, mustard dash-dot-dot-dot line; 0.40, dash-dot line. The dotted vertical lines represent the location of the 2^{nd} harmonic impurity resonant layer from Eq.2.

are sharply localized near the 2^{nd} harmonic impurity resonant layer for the values of H/H+D close the optimum from Eq.3. As H/H+D increases, the profiles broaden toward larger radius. The solid green curve for Ar^{16+} is reproduced in Fig.3 and aligns very nicely with the maximum pumpout just outside of the mid radius. A similar comparison can be made for the observed Ar^{17+} pumpout profile for the same discharge (Figs.1 and 3) and the results are displayed in Fig.20. Similar to what was seen in Fig.3, the calculated Ar^{17+} power absorption profile aligns well with the location of the observed maximum pumpout across the profile. These results show that indeed the short wavelength waves created by the mode conversion process interact strongly with the argon ions near the mode conversion regime. The correlation of the argon absorption *vs.* H concentration, and the power deposition and argon pumpout profiles, shows that RF wave interactions are the probable cause of the pumpout phenomena observed on C-Mod. To model further the behavior of the argon ions would need a transport code

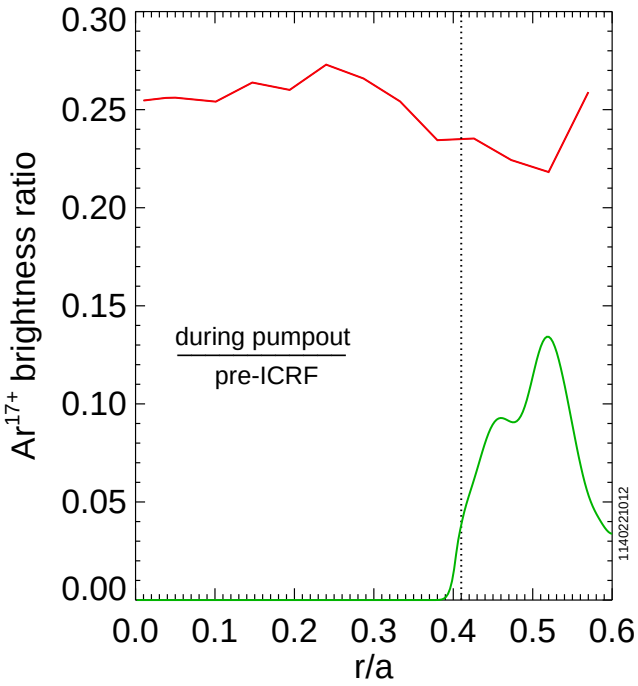

Figure 20: The ratio of the radial Ar^{17+} brightness profiles during the pumpout and before the ICRF for the discharge of Fig.1. The dotted vertical line indicates the location of the Ar^{17+} 2^{nd} harmonic resonant layer and the green curve represents the calculated power absorption profile for Ar^{17+} ions from Fig.19 with H/H+D = 0.31.

together with a Fokker-Planck RF code, and this is beyond the scope of the current study.

Unfortunately, as was mentioned above and shown in Table 1, the D(H) heating scheme is not particularly useful in pumping out very high Z impurities, since the high fractions of H required are not conducive to efficient heating. In future reactors like SPARC, a primary ICRF heating scheme will be with a ^{3}He minority in D-T plasmas. Similar to the D(H) case, the ideal ^{3}He minority fraction is in the interval from 5-10%. Fortunately in this range of ^{3}He minority concentration, there is substantial power absorption by highly charged tungsten ions, and potential W pumpout can be explored. TORIC simulations have been carried out for a plasma similar to the SPARC primary reference discharge with R_0 = 1.85 m, a = 0.57 m, B_T = 12.2 T, I_p = 8.7 MA, $T_i(0)$ = $T_e(0)$ = 10 keV, $n_e(0)$ = 5e20/m^3) [33]. The ICRF frequency is 120 MHz, near the ^{3}He fundamental cyclotron and tritium 2$^{\rm nd}$ harmonic resonances close to the plasma center. ^{3}He minority heating and T 2$^{\rm nd}$ harmonic heating will be the main mechanisms on SPARC. In the TORIC simulations, antenna toroidal numbers of n_ϕ = +36 and -36 were employed, with corresponding indices of refraction $k_\parallel \sim \pm$15/m, near the peak of the SPARC ICRF 4-strap antenna spectra [34]. Unlike the simple Eqs.1-3, with D, T and ^{3}He together, the ion-ion hybrid location is more complicated, but generally, with increased ^{3}He concentration level, the layer moves from near the ^{3}He fundamental cyclotron resonance layer at the plasma center towards the HFS, and ends near the D cyclotron resonance layer. In SPARC plasmas, mode conversion can happen for a moderate level of ^{3}He and still not affect the general power absorption. When the MC layer location is near the 2$^{\rm nd}$ harmonic resonance of argon-like W^{56+}, strong interactions can happen. An example is shown in Fig.21.

Shown in Fig.22 is the power fraction to W^{56+} ions as a function of ^{3}He concentration. While the maximum power is for 5% ^{3}He, there is substantial absorption up to 10%. The W^{56+} concentration is assumed to be 5e-5. For different ^{3}He concentrations, while keeping T at 40%, D is varied following the ^{3}He concentration for charge neutrality. The 2$^{\rm nd}$ harmonic resonance for W^{56+} is at X = -11.9 cm and the mode conversion layer for 10% ^{3}He is at X = -10.4 cm. (Caveat: the points for ^{3}He $\leq$ 5% may not be directly comparable with other points. In the scan, the ^{3}He ion temperature is kept constant at the same background temperature of 10 keV, but in reality, it would probably be at a much higher temperature so that the TORIC computation likely underestimates the power to ^{3}He ions and overestimates the power to W ions.)

This tungsten power absorption is selective for a very narrow range of charge states, as is shown in Fig.23, for a case with 40% D, 10% ^{3}He and 40% T. Each run uses a different W charge state and the tungsten concentration is assumed to be 5e-5. When the 2$^{\rm nd}$ harmonic resonance is close to the MC layer, for W^{55+} and W^{56+}, the power absorption can be significant. Argon-like W^{56+} is of particular interest since, because of the closed shell, it exists over a larger radial range and will be present in the core of high performance SPARC discharges with high electron temperatures. These results suggest an exciting possiblility for selective pumpout of tungsten by ICRF waves in a very attractive heating scheme. However, expulsion of high energy tungsten ions to plasma facing components could potentially lead to self sputtering, so this eventuality needs to be explored.

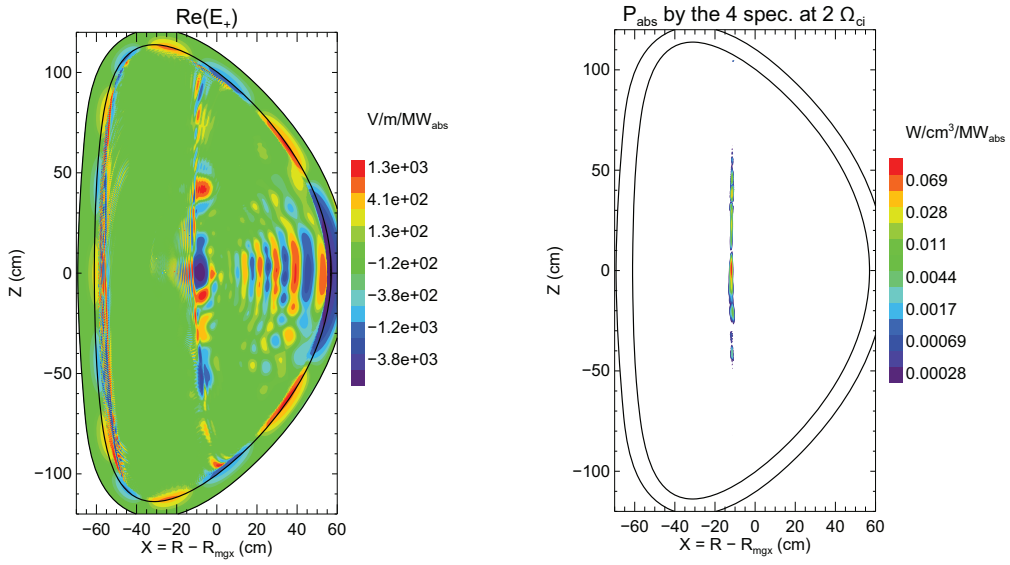

Figure 21: The calculated contours of the real parts of the electric field component E_+ (left) and power absorption for W^{56+} (right) for a SPARC D-T (^{3}He) discharge with trace tungsten. The MC layer is at X = -10.5 cm and the W^{56+} second harmonic is at -11.9 cm.

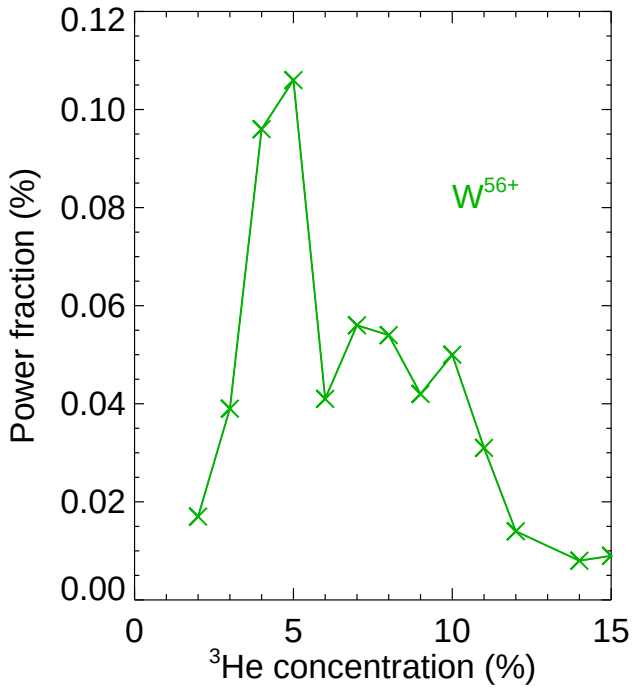

Figure 22: The power fraction absorbed by W^{56+} ions as a function of ^{3}He concentration in D-T 4 ion simulations of SPARC plasmas.

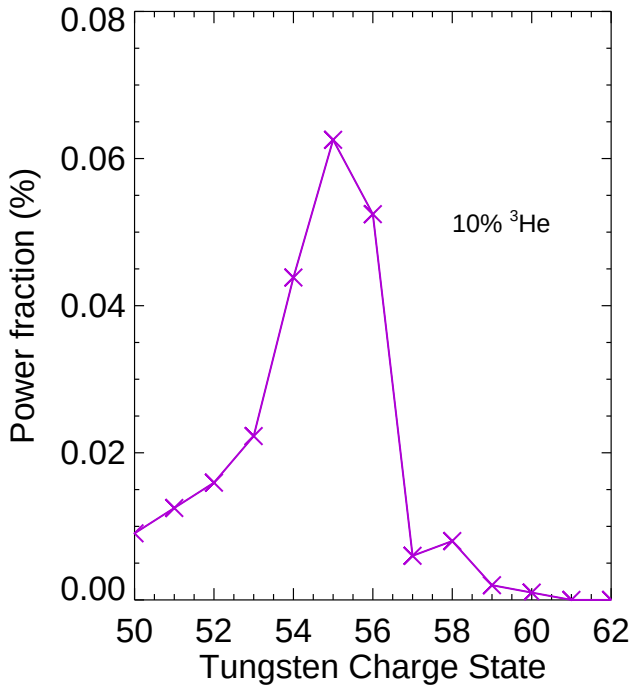

Figure 23: The power absorption as a function of tungsten charge state for 10% ^{3}He in SPARC D-T plasmas.

6. Summary

In summary, pumpout of argon ions by ICRF waves has been observed in C-Mod deuterium L- and I-mode plasmas that had a substantial hydrogen fraction. The effect is manifested by a reduction of core argon x-ray brightness up to a factor of 90% on time scales of tens of milliseconds following injection of ICRF power. For Ar^{16+}, the pumpout is strongest for hydrogen minority concentrations between 0.25 and 0.4, when the ICRF waves are not expected to result in minority heating. Maximum pumpout of Ar^{17+} occurs for slightly lower values of H/D. The magnitude of the argon pumpout is independent of ICRF power above an apparent threshold of $\sim$500 kW, independent of electron density and appears to decrease as the plasma current is increased. Modeling with the TORIC code suggests that the pumpout process occurs when the H/D mode conversion layer overlaps with the 2^{nd} harmonic impurity resonance layer. Very good agreement is found between calculations and the observed pumpout as a function of hydrogen minority concentration, as well as the radial dependence of the effect. Potential application as a tungsten control tool in reactors with ^{3}He minority heating in D-T plasmas has been discussed.

7. Acknowledgements

The authors appreciate enlightening discussions with R. Granetz, A. Hubbard, J.Hughes, J. Irby, P. Bonoli, R. Wilson, B. Grierson and D. Ernst, and thank the Alcator C-Mod operations and ICRF groups for expert running of the tokamak. Work supported at MIT by DoE Award DE-SC0014264.

References

[1] J.E.Rice *et al.*, 2002 *Nucl. Fusion* **42** 510.

[2] M.Valisa *et al.*, 2011 *Nucl. Fusion* **51** 033002.

[3] A.Kallenbach *et al.*, 2009 *Nucl. Fusion* **49** 045007.

[4] B.A.Grierson *et al.*, 2018 *Phys. Plasmas* **25** 022509.

[5] T.W.Petrie *et al.*, 2019 *Nucl. Mater. Eng.* **19** 267.

[6] T.Odstrčil *et al.*, 2020 *Phys. Plasmas* **27** 082503.

[7] TFR Group, 1982 *Nucl. Fusion* **22** 956.

[8] E.S.Marmar *et al.*, 2007 *Fusion Sci. Technol.* **51** 261.

[9] M.Greenwald *et al.*, 2014 *Phys. Plasmas* **21** 110501.

[10] P.T.Bonoli *et al.*, 2007 *Fusion Sci. Technol.* **51** 401.

[11] M.Porkolab *et al.*, 1998 *Plasma Phys. Control. Fusion* **40** A35.

[12] T.E.Tutt, 1999, "H_α/D_α Spectroscopy on Alcator C-Mod", S.M. thesis, M.I.T.

[13] J.E.Rice *et al.*, 1987 *Phys. Rev. A* **35** 3033.

[14] E.S.Marmar *et al.*, 1986 *Phys. Rev. A* **33** 774.

[15] A.Ince-Cushman *et al.*, 2008 *Rev. Sci. Instrum.* **79** 10E302.

[16] M.L.Reinke *et al.*, 2012 *Rev. Sci. Instrum.* **83** 113504.

[17] J.E.Rice *et al.*, 1995 *Phys. Rev. A* **51** 3551.

[18] M.L.Reinke *et al.*, 2010 *Rev. Sci. Instrum.* **81** 10D736.

[19] J.E.Rice *et al.*, 2015 *Nucl. Fusion* **55** 033014.

[20] B.Lipschultz *et al.*, 2001 *Nucl. Fusion* **41** 585.

[21] D.G.Whyte *et al.*, 2010 *Nucl. Fusion* **50** 105005.

[22] A.E.Hubbard *et al.*, 2016 *Nucl. Fusion* **56** 086003.

[23] T.H.Stix, 1962 "The Theory of Plasma Waves", McGraw-Hill, New York.

[24] P.Rodriguez-Fernandez *et al.*, 2020 *J. Plasma Phys.* **86** 865860503.

[25] R.Neu *et al.*, 1997 *J. Phys. B* **30** 5057.

[26] J.R.Wilson *et al.*, 1998 *Phys. Plasmas* **5** 1721.

[27] M.Brambilla, 1998 *Nucl. Fusion* **38** 1805.

[28] M.Brambilla, 1999 *Plasma Phys. Control. Fusion* **41** 1.

[29] M.Porkolab, 1994 "Plasma heating by fast waves in tokamaks" in AIP Conference Proceedings (ed. T.H.Stix & N.J.Fisch), vol. 314, p. 99. American Institute of Physics.

[30] E.Nelson-Melby *et al.*, 1990 *Phys. Rev. Lett.* **90** 155004.

[31] Y.Lin *et al.*, 2003 *Plasma Phys. Control. Fusion* **45** 1013.

[32] Y.Lin *et al.*, 2005 *Plasma Phys. Control. Fusion* **47** 1207.

[33] A.Creely *et al.*, 2020 *J. Plasma Phys.* **86** 865860502.

[34] Y.Lin *et al.*, 2020 *J. Plasma Phys.* **86** 865860506.